Supporting information

A Dual-Functional Sodium Alginate-Poly Zinc Acrylate Hydrogel Electrolyte for Enhanced Stability of Aqueous Zinc-Ion Batteries

Jiale Chen,‡[a] Rongchang Yang,‡[a] Yuchao Chen,[a] Dongshu Liu,[a] Shibo Meng,[a] Wenxian Liu,[a] Fangfang Wu,[a] Wenhui Shi,*[b] and Xiehong Cao*[a]

[a] College of Materials Science and Engineering, State Key Laboratory of Advanced Separation Membrane Materials, Zhejiang University of Technology, 18 Chaowang Road, Hangzhou, Zhejiang 310014, P. R. China.
E-mail: gcscaoxh@zjut.edu.cn.
[b] College of Chemical Engineering, State Key Laboratory of Advanced Separation Membrane Materials, Zhejiang University of Technology, 18 Chaowang Road, Hangzhou, Zhejiang 310014, P. R. China.
E-mail: shiwh@zjut.edu.cn

Experimental Section

Synthesis of PAZ-S and SA gel electrolytes

Sodium alginate (SA, Rhawn, ≥90% purity, 0.25g) was uniformly dispersed in 10 mL of deionized water. Acrylic acid (AA, Sinopharm Group, AR grade) was introduced at a volumetric ratio of $V(H_2O):V(AA) = 10:3.6$. Zinc polyacrylate (PAZ) precursor solution was obtained by dissolving 2.35 g ZnO powder (Aladdin, 99.8%) into the AA solution under continuous stirring for 4 h. The resultant suspension was centrifuged, and the supernatant was collected. Subsequently, 15 mg N-N 'methylene bisacrylamide (MBAA, Aladdin, 99%) and 110 mg ammonium persulfate (APS, Aladdin, 98%) were added as crosslinker and initiator, respectively, followed by 1h ultrasonication.

The SA dispersion was cast into a mold and immersed in PAZ precursor for 24 h. Hydrogel formation was achieved through thermal polymerization at 80 °C for 10 min. The obtained PAZ-S composite hydrogel was then equilibrated in 2 mol L^{-1} $ZnSO_4$ and 0.2 mol L^{-1} $MnSO_4$ electrolyte solution with electrolyte renewal every 8 h.

SA hydrogel was poured into the mold and soaked in 2 mol L^{-1} $ZnSO_4$ and 0.2 mol L^{-1} $MnSO_4$ electrolyte solution with electrolyte renewal every 8 h.

Synthesis of MnO_2 cathode

A homogeneous solution containing 405.648 mg $MnSO_4 \cdot H_2O$ in 20 mL deionized water was mixed with 948.18 mg $KMnO_4$ dissolved in 40 mL deionized water. The mixture was hydrothermally treated in a 100 mL Teflon-lined autoclave at 160°C for 12 h. The resultant precipitate was collected via centrifugation, sequentially washed with DIW and ethanol (3 cycles each), and vacuum-dried at 60°C for 12 h.

Material Characterization.

Crystalline structures were analyzed by X-ray diffraction (XRD, PANalytical X'Pert PRO, Cu Kα $\lambda = 0.1541$ nm). Morphological features were examined using field-emission SEM (FESEM, Hitachi SU-8010) and transmission electron microscopy (TEM, Philips-FEI Tecnai G2 F30 S-Twin) with energy-dispersive X-ray spectroscopy (EDS). Chemical states were probed via X-ray photoelectron spectroscopy (XPS, Shimadzu Kratos Axis Ultra-DLD). Functional groups were identified by Fourier-transform infrared spectroscopy (FT-IR, Nicolet 6700, Thermo Fisher). Surface topography was mapped using 3D laser scanning microscopy (LSM700, Zeiss).

Thermogravimetry analysis (TGA) was carried out on a HITACHI STA300 analyzer in 30-800°C in a dynamic N_2 atmosphere with a heating rate of 10°C/min.

Electrochemical Measurements

CR2032 coin cells were assembled in ambient conditions. Cyclic voltammetry (CV, 0.8–1.85 V vs. Zn/Zn^{2+}) and electrochemical impedance spectroscopy (EIS, 100 kHz–0.01 Hz) were conducted on a CHI760E workstation. Symmetric Zn//Zn and full-cell cycling tests were performed using a Neware BTS-4000 system.

Cathodes were prepared by homogenizing MnO_2, acetylene black (ECP), and polyvinylidene fluoride (PVDF) binder in N-methyl-2-pyrrolidone (NMP) at an 8:1:1 mass ratio.

Ionic conductivity (σ) was determined by AC impedance using stainless steel blocking electrodes (area = 1.766 cm^2), calculated as $\sigma = L/(R\times S)$, where L (cm), R (Ω), and S (cm^2) represent electrolyte thickness, bulk resistance, and electrode area, respectively. Zinc-ion transference number (t_{Zn2+}) of the PAZ-S was measured by the potentiostatic polarization method and calculated by the following Bruce-Vincent equation:

$$t_{Zn^{2+}} = \frac{I_S\ (\Delta V - I_0 R_0)}{I_0\ (\Delta V - I_S R_S)}$$

where I_0 and Is represent the currents at the initial and steady states, respectively. R_0 and Rs represent the interfacial resistances before and after polarization, respectively. The results were obtained by performing electrochemical impedance spectroscopy (EIS) before and after chronoamperometry measurements. The frequency of EIS ranged from 100000 to 0.1 Hz with a voltage of 10 mV. The current–time profile was obtained by applying a voltage of 10 mV for 1 h.

Pouch cell assembly

Pouch cells were constructed in a $Zn//MnO_2$ sandwich configuration. Zinc foil (anode) and MnO_2 cathode (active mass loading ≈1.4 mg cm^{-2}, geometric area = 3.5 × 3.5 cm^2) were laminated onto opposing sides of the PAZ-S hydrogel electrolyte under controlled pressure.

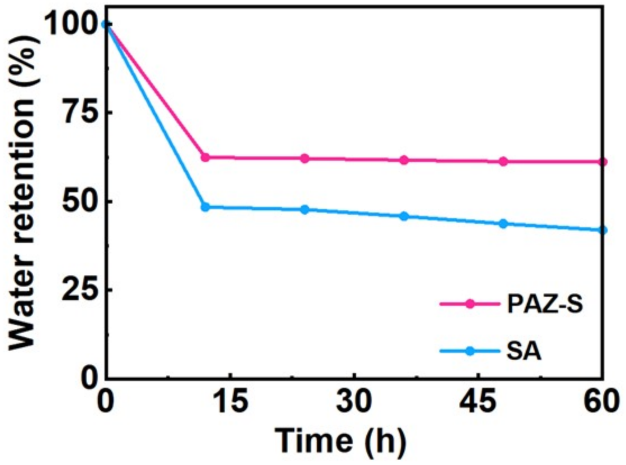

Figure S1. The water retention capabilities of SA and PAZ-S hydrogels.

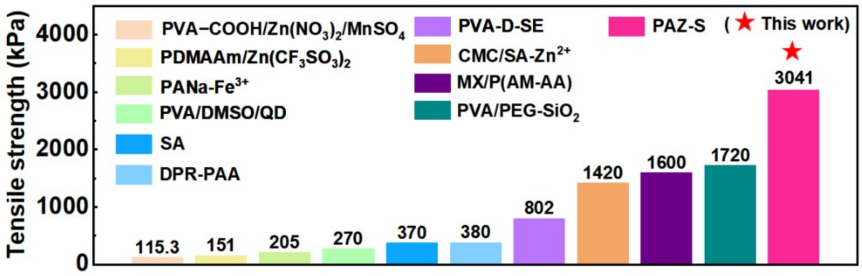

Figure S2. Comparison of tensile strength of PAZ-S hydrogel with other reports.

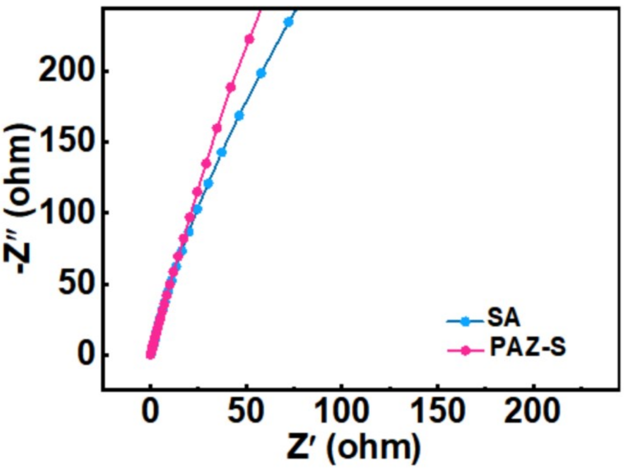

Figure S3. AC impedance of the SA and PAZ-S gel electrolytes.

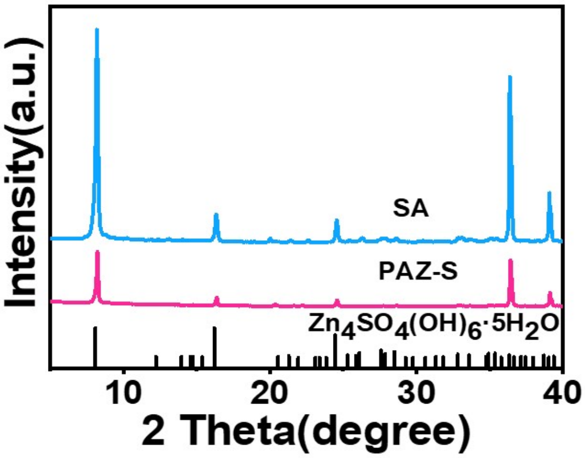

Figure S4. XRD patterns comparison of Zn anodes.

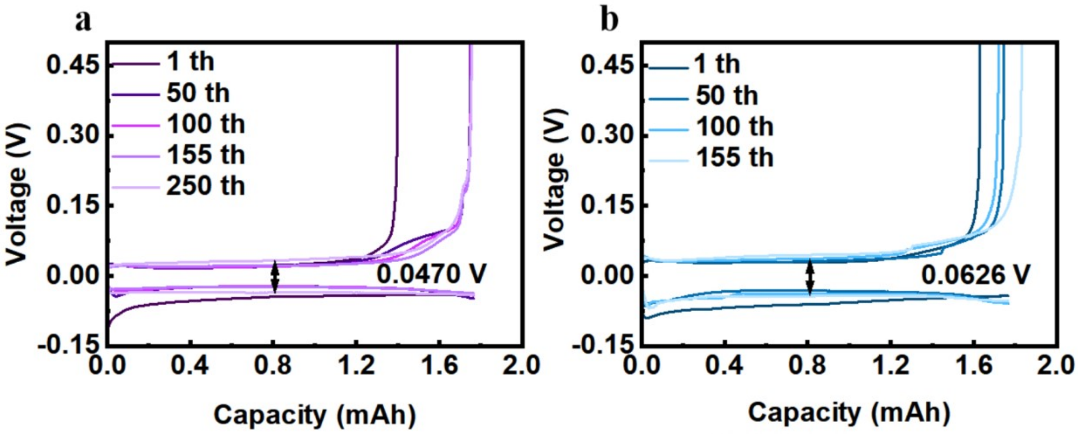

Figure S5. Voltage profiles of the (a) PAZ-S electrolyte and (b) SA electrolyte at 1 mA cm^{-2} with the capacity limited to 1 mA h cm^{-2}.

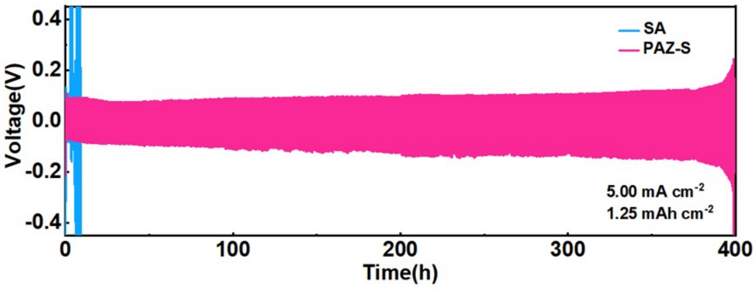

Figure S6. Zn stripping/plating performances of Zn/PAZ-S/Zn and Zn/SA/Zn symmetric batteries under 5 mA cm^{-2}/1.25 mA h cm^{-2}.

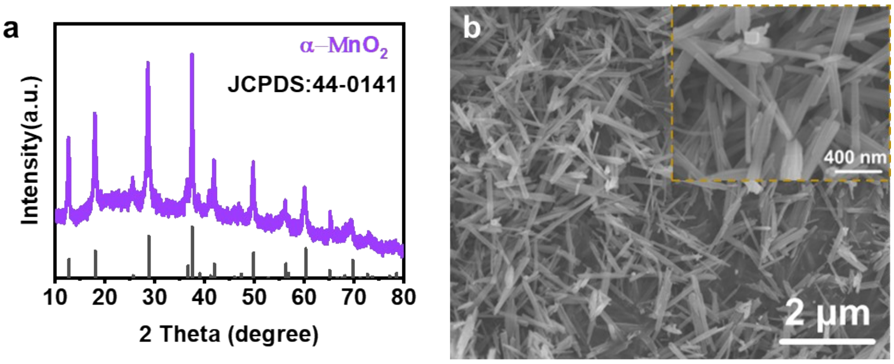

Figure S7. (a) XRD and (b) SEM images of MnO_2.

As shown in Figure S7a, the XRD pattern of the synthesized MnO_2 matches the standard diffraction peaks of α-MnO_2 (PDF#44-0141), confirming the successful synthesis of α-MnO_2. SEM images in Figure S7b further reveal that the synthesized MnO_2 exhibits a nanorod-like structure.

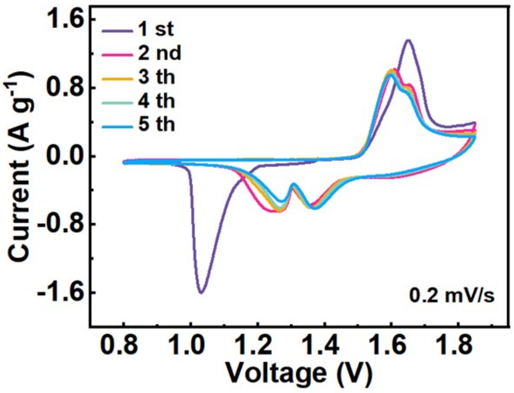

Figure S8. CV curves of Zn/PAZ-S/MnO_2 cell.

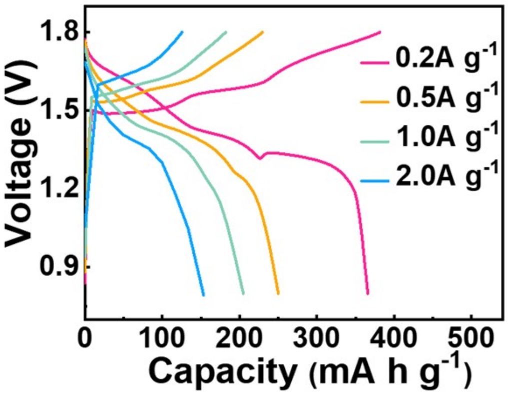

Figure S9. GCD curves at current densities ranging from 0.2 to 2 A g^{-1} of Zn/PAZ-S/MnO_2 cell.

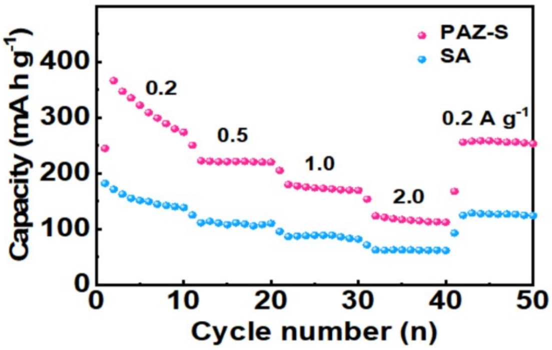

Figure S10. Rate performance of Zn/PAZ-S/MnO_2 cell and Zn/SA/MnO_2 cell.

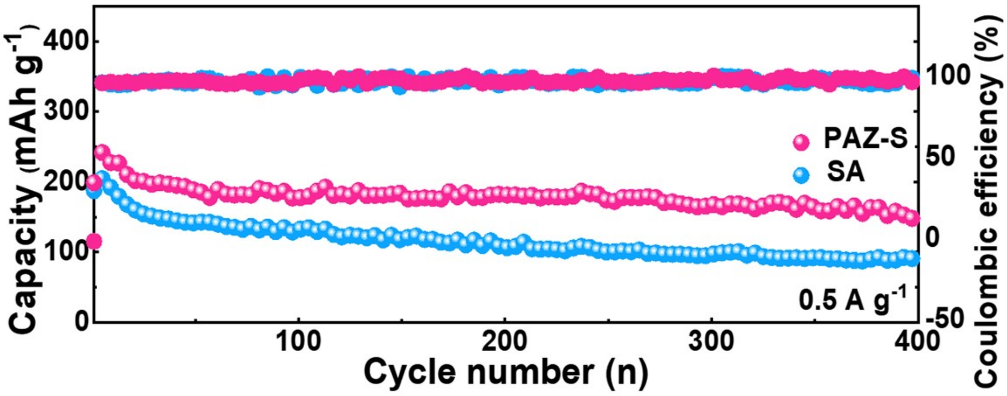

Figure S11. Cycling stability at a current density of 0.5 A g^{-1} of Zn/PAZ-S/MnO_2 cell.

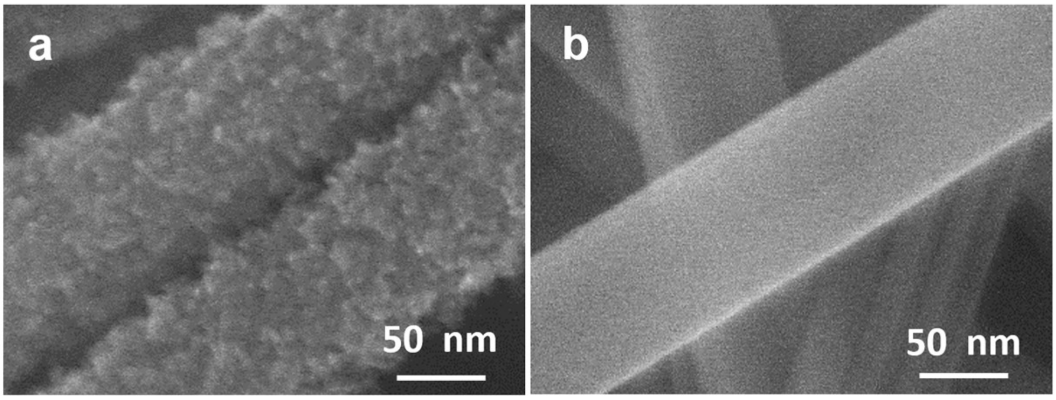

Figure S12. Post-cycling cathode morphology in (a) the PAZ-S system and (b) the SA system after 50 cycles.

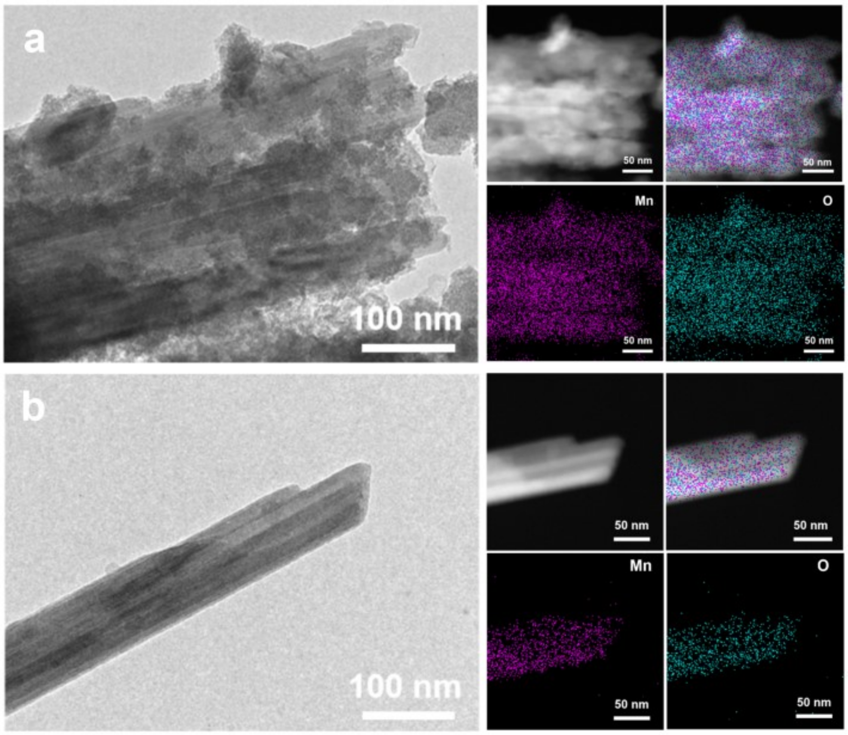

Figure S13. TEM images and the corresponding EDX mappings of MnO_2 cathodes with (a) PAZ-S and (b) SA hydrogel electrolyte after 50 cycles at 0.5 A g^{-1}.

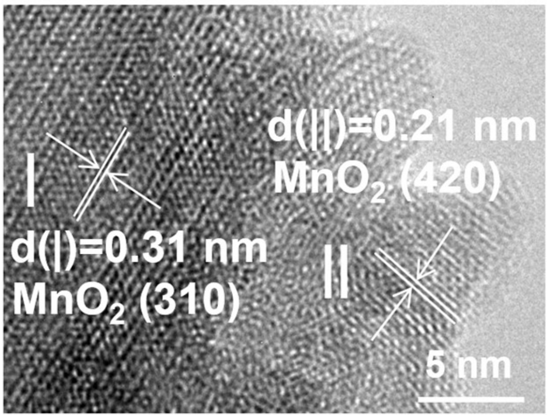

Figure S14. High-resolution TEM analysis of MnO_2 cathode with PAZ-S hydrogel electrolyte after 50 cycles at 0.5 A g^{-1}.

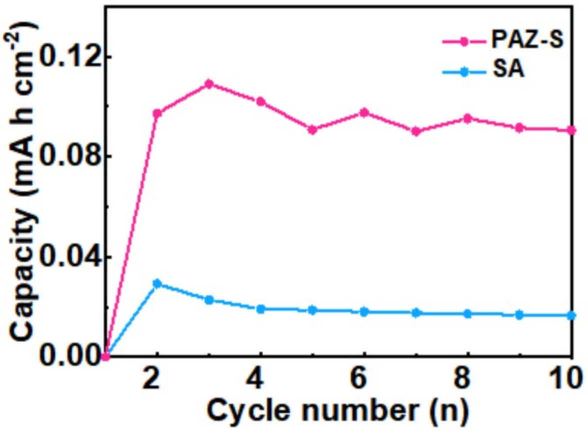

Figure S15. Capacity contribution of Zn//CC cell cycled with PAZ-S and SA hydrogel electrolytes.

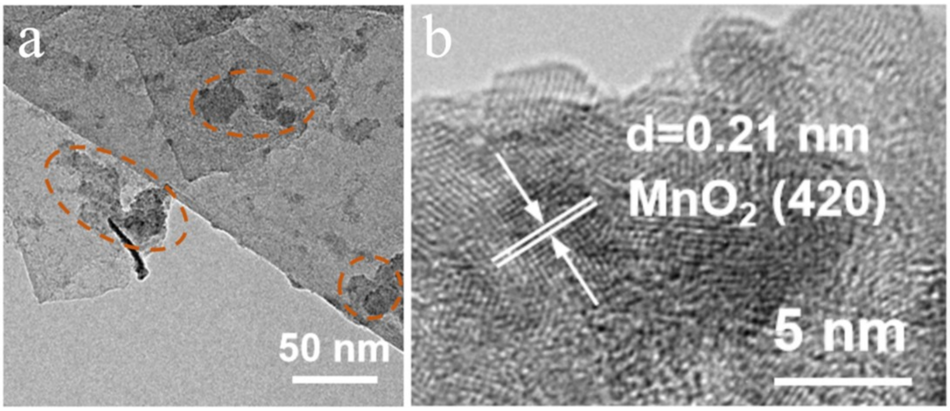

Figure S16. (a) TEM and (b) HRTEM image of PAZ-S deposited material on carbon cloth after 10 cycles of Zn/PAZ-S/CC cell.

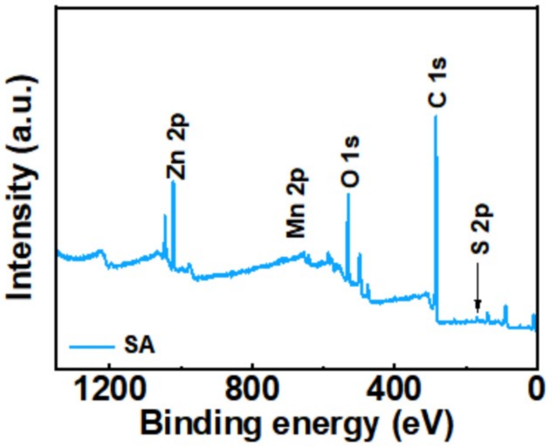

Figure S17. XPS results of carbon cloth after 10 cycles of Zn/SA/CC cell.

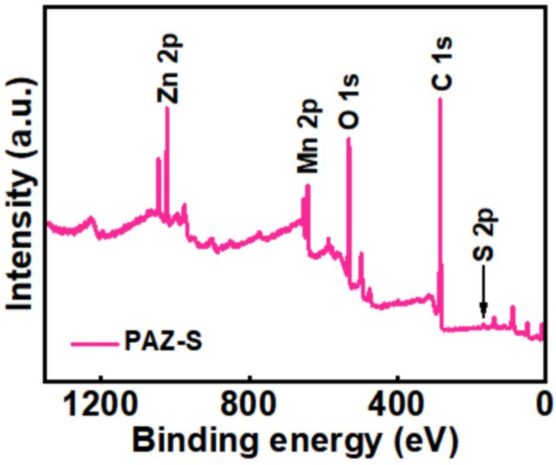

Figure S18. XPS results of carbon cloth after 10 cycles of Zn/PAZ-S/CC cell.

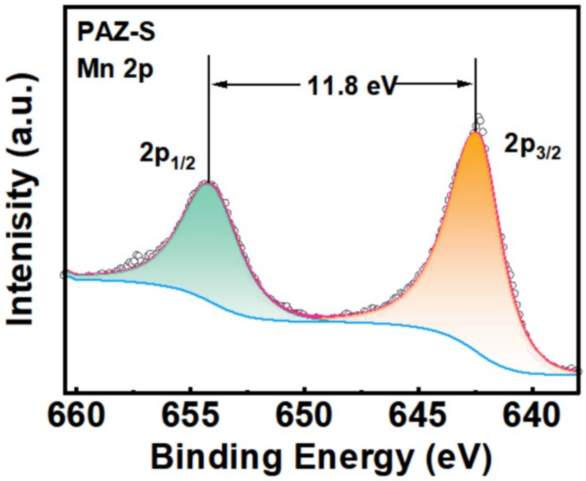

Figure S19. XPS analysis: Mn 2p spectra and high-resolution Mn 2p spectrum after 10 cycles with PAZ-S.

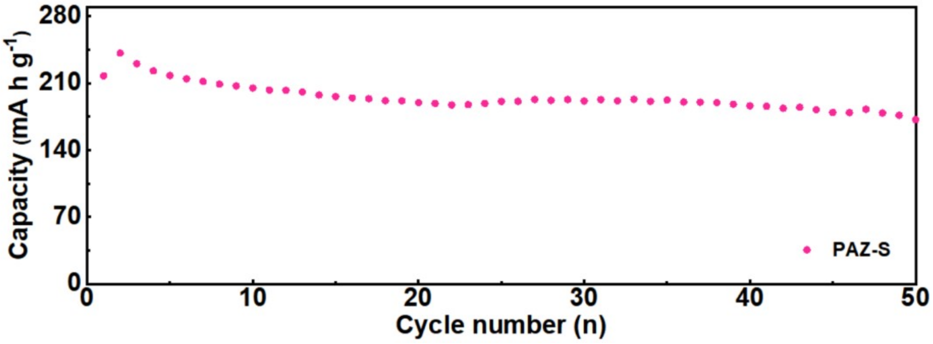

Figure S20. Cycling stability of the soft pack cell at a current density of 0.2 A g^{-1}.

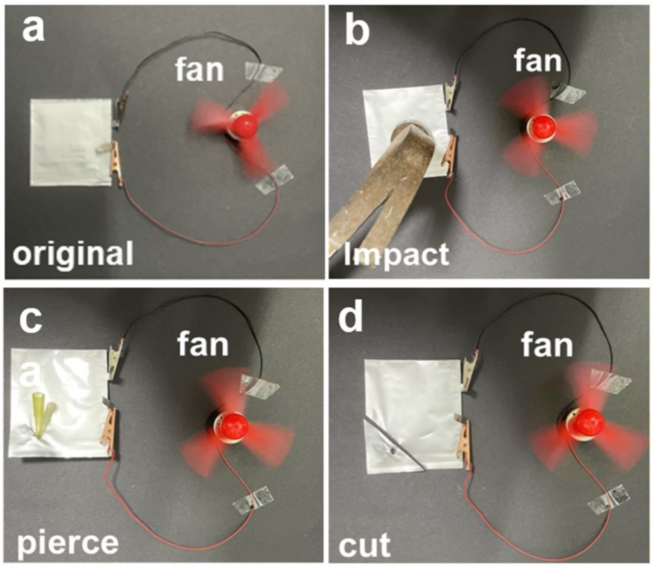

Figure S21. Safety validation under (a) original and mechanical abuse: (b) impact, (c) piercing and (d) cutting.

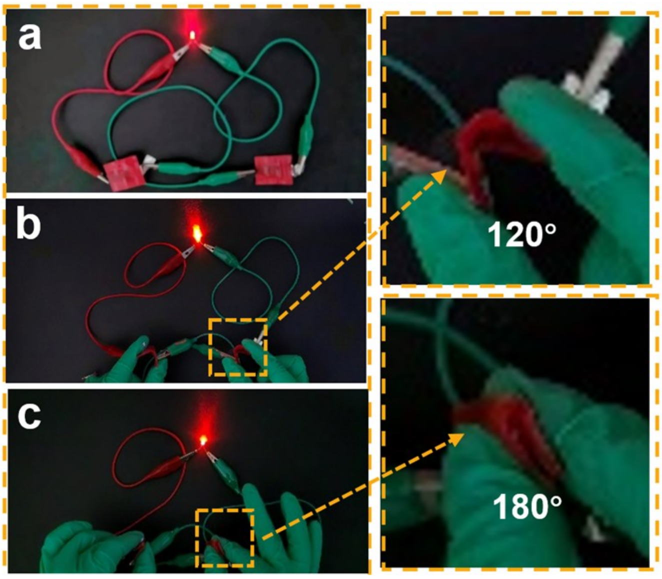

Figure S22. Functional tests showing the LED operation with bending at angles of (a) 0°, (b) 120° and (c) 180°.

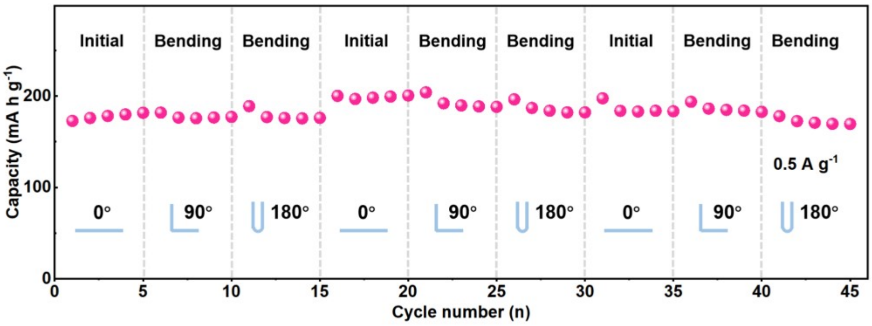

Figure S23. Cycling performance of the flexible device assembled with PAZ-S hydrogel electrolyte under different bending angles.

Figure S24. Functional tests showing smartwatch powering capability.

Table S1. Comparison of tensile strength of PAZ-S hydrogel with other reports.

Reference	**Tensile strength (kPa)**	**Hydrogel electrolyte**
1	115.3	PVA−COOH/$Zn(NO_3)_2$/$MnSO_4$
2	151	PDMAAm/$Zn(CF_3SO_3)_2$
3	205	PANa-Fe^{3+}
4	270	PVA/DMSO/QD
This work	370	SA
5	380	DPR-PAA
6	802	PVA-D-SE
7	1420	CMC/SA-Zn^{2+}
8	1600	MX/P(AM-AA)
9	1720	PVA/PEG-SiO_2
This work	3041	PAZ-S

Table S2 Comparison of ionic conductivity of PAZ-S hydrogel with other reports listed in Figure 2g.

Reference	**Ionic conductivity (mS cm^{-1})**	**Gel electrolyte**
7	2.08	CMC/SA-Zn^{2+}
10	5.51	CS-PASP-ZnSO$_4$
11	9.52	CA
12	10.7	GG
13	10.98	PAM+45%trehalose
14	11	Gum Arabic
15	11	HCCE
16	12.3	CAG
17	13.3	CNF/PAM
18	13.3	PAM-DMSO-CNF
19	14	PVA–SA–acetate
20	14.6	Xanthan Gum
21	15.6	PAMPSZn
22	17.4	C-PVA/PAN
23	17.6	GE-g-PAM
24	18.86	PSX
25	19.834	PAM+5%DMC [18]
26	20.7	MMT-PAM [19]
This work	20.75	SA
27	22.02	PAM/MWCNT
This work	24.01	PAZ-S
28	25.37	GG/SA/EG

Reference

1.Q. Li, X. Cui and Q. Pan, *ACS Appl. Mater. Interfaces*, 2019, **11**, 38762-38770.

2. H. Li, Y. Liu, Z. Chen, Y. Yang, T. Lv and T. Chen, *J. Colloid Interface Sci.,* 2023, **639**, 408-415.

3.Y. Huang, J. Liu, J. Wang, M. Hu, F. Mo, G. Liang and C. Zhi, Angew. Chem., 2018, **57**, 9810-9813.

4.J Du, X Zhan, Y Xu, K Diao, D Zhang and S Qin, *J Mater Sci Technol.*, 2025, **212**, 251-258.

5.J Xu, Y Zhu, Q Gui, S Sun, P Zhao, L Mao and T Luo, *Small*, 2025, **21**, 2500124

6.J Kang, Z Jiang and L Wen, *Adv. Funct. Mater.*, 2025, 2422566

7.Y Yang, L Shi, Y Wu, Z Chen, X Zhu, L Du and Y Wang, *Chem. Eng. J.*, 2024, **484,** 149780.

8.AC Radjendirane, S Ramasamy, SP Rajendra, G Murali, I In, SJ Lee and S Angaiah,

Electrochimica Acta, 2025,**531**, 146368.

9.F Wan, K Hu, R Liu, S Zhang, S Li, Y Lei, D Yang, C Wang, Y Xia and W Chen, *Chem. Comm.*, 2024, **60**, 7220-7223.

10. H. Lu, J. Hu, X. Wei, K. Zhang, X. Xiao, J. Zhao, Q. Hu, J. Yu, G. Zhou and B. Xu, *Nat. Commun.*, 2023, **14**, 4435.

11. J.-H. Park, S. H. Park, D. Joung and C. Kim, *Chem. Eng. J.*, 2022, **433**, 133532.

12. Y. Huang, J. Zhang, J. Liu, Z. Li, S. Jin, Z. Li, S. Zhang and H. Zhou, *Mater. Today Energy*, 2019, **14**, 100349.

13. S. Yang, Q. Wu, Y. Li, F. Luo, J. Zhang, K. Chen, Y. You, J. Huang, H. Xie and Y. Chen, *Angew. Chem.*, 2024, **136**, e202409160.

14. K. Wu, J. Cui, J. Yi, X. Liu, F. Ning, Y. Liu and J. Zhang, *ACS Appl. Mater. Interfaces*, 2022, **14**, 34612-34619.

15. J. Gao, X. Xie, S. Liang, B. Lu and J. Zhou, *Nano-Micro Lett.*, 2021, **13**, 1-12.

16. J. Zhou, R. Zhang, R. Xu, Y. Li, W. Tian, M. Gao, M. Wang, D. Li, X. Liang and L. Xie, *Adv. Funct. Mater.*, 2022, **32**, 2111406.

17. D. Wang, H. Li, Z. Liu, Z. Tang, G. Liang, F. Mo, Q. Yang, L. Ma and C. Zhi, *Small*, 2018, **14**, 1803978.

18. S. Huang, S. He, Y. Li, S. Wang and X. Hou, *Chem. Eng. J.*, 2023, **464**, 142607.

19. L. Ma, X. Liu, J. Fan, X. Yu, L. Cao and C. Zhao, *Mater. Horiz.*, 2025, **12**, 2736-2744.

20. S. Zhang, N. Yu, S. Zeng, S. Zhou, M. Chen, J. Di and Q. Li, *J. Mater. Chem. A*, 2018, **6**, 12237-12243.

21. J. Cong, X. Shen, Z. Wen, X. Wang, L. Peng, J. Zeng and J. Zhao, *Energy Storage Mater.*, 2021, **35**, 586-594.

22. H. Xia, W. Zhang, C. Miao, H. Chen, C. Yi, Y. Shang, T. Shui, X. Cao, J. Liu and S.-Z. Kure-Chu, *Energy Environ. Sci.*, 2024, **17**, 6507-6520.

23. H. Li, C. Han, Y. Huang, Y. Huang, M. Zhu, Z. Pei, Q. Xue, Z. Wang, Z. Liu and Z. Tang, *Energy Environ. Sci.*, 2018, **11**, 941-951.

24. C. Fu, Y. Wang, C. Lu, S. Zhou, Q. He, Y. Hu, M. Feng, Y. Wan, J. Lin and Y.

Zhang, *Energy Storage Mater.*, 2022, **51**, 588-598.
25. Y. Zhang, Y. Li, K. Chen, F. Luo, Q. Xu, J. Huang and H. Xie, *Chem. Eng. J.*, 2025, **511**, 162164.
26. S. Ji, J. Qin, S. Yang, P. Shen, Y. Hu, K. Yang, H. Luo and J. Xu, *Energy Storage Mater.*, 2023, **55**, 236-243.
27. F. Luo, S. Yang, Q. Wu, Y. Li, J. Zhang, Y. Zhang, J. Huang, H. Xie and Y. Chen, *Energy Environ. Sci.*, 2024, **17**, 8570-8581.
28. J. Wang, Y. Huang, B. Liu, Z. Li, J. Zhang, G. Yang, P. Hiralal, S. Jin and H. Zhou, *Energy Storage Mater.*, 2021, **41**, 599-605.